Optimizing the coupling efficiency of spontaneous parametric down-conversion photon pairs into single-mode fibers

Nicolas Schwaller,[1,2] Geobae Park,[1] Ryo Okamoto,[1,3] and Shigeki Takeuchi[1,*]

[1]*Department of Electronic Science and Engineering, Kyoto University, Kyoto Daigaku-Katsura, Nishikyo-ku, Kyoto 615-8510, Japan*

[2]*Institute of Physics, Swiss Federal Institute of Technology (EPFL), CH-1015 Lausanne, Switzerland*

[3]*PRESTO, Japan Science and Technology Agency, 4-1-8 Honcho, Kawaguchi, Saitama 332-0012, Japan*

(Received 14 June 2022; accepted 30 September 2022; published 28 October 2022)

Both correlated-mode coupling efficiency and photon pair flux (brightness) of spontaneous parametric down-conversion (SPDC) coupled into single-mode fibers are key parameters for various quantum information science applications. We present an experimental investigation on the optimization of the correlated-mode coupling efficiency and the brightness of frequency-degenerated SPDC photon pairs into single-mode optical fibers. Using photon pairs generated from a type-I phase-matched bulk β-barium borate crystal pumped by a continuous-wave laser, we carefully evaluated both the correlated-mode coupling efficiency and the brightness of SPDC light coupled to a single-mode optical fiber, while continuously changing the focusing of the pump and collection modes, experimenting with Rayleigh lengths from 3 to 280 (for the pump) and 0.2 to 20 (for the collection) times the crystal length. The measured data suggest that the correlated-mode coupling efficiency can be close to unity for any pump focus, however, the optimal Rayleigh length of the collection mode depends on the pump focus parameter, and the brightness can be increased by tightening the pump focus, provided that the Rayleigh length of the collection mode is precisely adjusted. A maximal correlated-mode coupling efficiency of $99.0 \pm 1.3\%$ was experimentally achieved. These results will be useful for photonic quantum science and technology using SPDC sources with high heralding efficiencies.

DOI: 10.1103/PhysRevA.106.043719

I. INTRODUCTION

Spontaneous parametric down-conversion (SPDC) is an optical nonlinear process in which a pump photon is converted into a pair of daughter photons (called signal and idler). The first experimental evidence of this process dates back to 1967 [1], and it soon gave rise to various applications [2–4]. The strong correlations between photons produced by SPDC [5] were harnessed to develop robust and high-flux sources of entangled photon pairs that function at room temperature, providing important advances in quantum technologies, such as quantum cryptography [6,7], quantum imaging [8,9], and quantum computing [10,11]. The quest for efficient coupling of SPDC photon pairs into single-mode (SM) fibers is an essential step toward the successful application of photonic quantum solutions as SM fibers are ideal routes for transferring quantum information since they preserve the phase relations and spatial indistinguishability of the traveling photons [12]. After excluding misalignment of the optical path, losses due to aberrations and the limited transmission of optical elements, the coupling efficiency can still be heavily impacted by spatial mode mismatch between the emitted photons and the detection apparatus.

The metric designed to measure the degree of spatial mode matching is known as the correlated-mode coupling efficiency η_c, which is the probability for one photon to be coupled to the collection (or detection) mode, conditional on the other photon also being in its detection mode [13]. Maximizing η_c is key to improving the collection efficiency of heralded photon sources [14], which is itself essential to improve the performance of tasks based on correlated photon pairs, such as speed or signal-to-noise ratio.

Note that optimization of the collection of entangled photon pairs into single-mode fibers was carried out by matching the mode diameters of the pump and collection modes inside the crystal [15], however, a detailed study on the optimization of the correlated-mode coupling efficiency had been lacking. Recently, this topic has been studied mainly theoretically in previous works [16–19]. A thorough experimental study of the correlated-mode coupling efficiency into SM fibers of SPDC photon pairs generated in a type-II quasi-phase-matching periodically poled potassium titanyl phosphate crystal was also performed by Dixon *et al.* [13]. In their work, they demonstrated that it is possible to reach an efficiency of $\eta_c = 97\% \pm 2\%$ if the experimental conditions are adjusted appropriately. In addition, they showed that their experimental results are consistent with the theory developed by Ref. [18]. However, the range of the collection mode focusing and pump mode focusing were limited and, thus, further experimental effort is desired for the verification of the theoretically predicted optimal condition experimentally.

In this paper, we intend to further experimentally optimize η_c for sources based on type-I phase matching (broadband photons), which is typical of the earliest SPDC experiments and still actively used [20] in tests of quantum theory

*takeuchi@kuee.kyoto-u.ac.jp

[21,22], generation of multiphoton parallel states [23–25], nonlinear interferometers [26] or two photon absorption techniques [27]. The crucial experimental parameters for optimizing the coupling of photon pairs into SM fibers are the focusing conditions [13,16–19]. Therefore, in order to perform a methodical analysis of the behavior of η_c as a function of the focusing, we built an experimental setup allowing independent and continuous variation of the waists of the pump and collection beams at the center of a 3-mm long β-barium borate (BBO) crystal. This enables experimentation with a large range of Rayleigh lengths, from 3 to 280 and 0.2 to 80 times the crystal length (containing the ranges investigated in Ref. [13]) for the pump and the detection beams, respectively. In this way, we could search for the optimal parameters to maximize η_c, pushing it up to $(99.0 \pm 1.3)\%$, while optimizing the brightness of the source. Our results suggest that the overall optimal condition is reached with a Rayleigh length equaling the crystal length for the collection beam, and a Rayleigh length about eight times longer for the pump beam. We also analyzed the deviations from theory-based predictions in our experimental results. An experimental investigation of η_c using type-I phase matching can also be found in Ref. [19]. However, their study was limited to individual measurements and did not show evidence of the existence of an optimal configuration. Here, we systematically study the dependence of η_c on excitation and collection geometry and show that nearly perfect mode matching can be obtained experimentally for collinear degenerate emission. We believe that the content of our report will be informative for future optimization of SPDC photon pair sources.

The remainder of this paper is organized as follows. Section II defines the correlated-mode coupling efficiency and its physical meaning. Section III presents the experimental method, and the results are discussed in Sec. IV.

II. CORRELATED-MODE COUPLING EFFICIENCY

Consider a pair of photons: given that one photon of the pair is emitted into the (single) detection mode of the fiber, η_c is the probability that the other is also successfully emitted into the detection mode. Pairs with only one photon in the detection mode are the cause of low η_c [17–19]. A representation of this effect is given in Fig. 1; in this example, the statistics indicate that a single photon has a chance of 80% to be coupled to the fiber and that in those cases, $\eta_c = 75\%$ of the time the paired photon will also be collected. We use the indices j, k to label the signal and idler spatial modes,

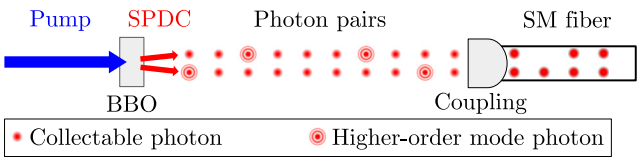

FIG. 1. SPDC photon pairs emitted in free space and coupled to single-mode fibers. Only the photons emitted in the detection mode, noted "0" in Eq. (2), can enter the fibers. In this example, from a total of ten pairs, six can be fully coupled to the fiber, and from ten single photons, only eight can be coupled, thus, $\eta_c = 6/8 = 0.75$.

respectively. We assume that different indices always imply orthogonal modes. Following the notation of Ref. [13], the state of two SPDC photons emitted in modes j and k is written as

$$|\psi(j,k)\rangle = \psi(j,k)\hat{a}_j^\dagger \hat{b}_k^\dagger |0\rangle , \tag{1}$$

where $\hat{a}_j^\dagger$ ($\hat{b}_k^\dagger$) is the creation operator for the field of the signal (idler) photon in mode j (k), and $|0\rangle$ is the vacuum state. Indexing the detection mode as mode 0 and summing over all the modes available to both photons (restricted by the conservation of orbital angular momentum), the state of the SPDC light reads

$$|\Psi_{\text{SPDC}}\rangle = C_{00}|\psi(0,0)\rangle + \sum_{j,k>0} C_{jk}|\psi(j,k)\rangle + \sum_{j>0} C_{j0}|\psi(j,0)\rangle + \sum_{k>0} C_{0k}|\psi(0,k)\rangle , \tag{2}$$

where the first term (coefficient C_{00}) represents pairs with both photons in the detection mode, $j,k = 0$, and the second one (coefficient C_{jk}) represents pairs with both photons in higher-order modes, $j,k > 0$. The two last terms (coefficients C_{j0} and C_{0k}) represent pairs in which only one photon is emitted in the detection mode, that is, $j = 0, k > 0$ or $j > 0, k = 0$. Note that we neglected multipair generation as the pump light is produced by a low-power continuous wave (cw) laser as well as any losses. Then, η_c can readily be expressed based on the coefficients of Eq. (2) as

$$\eta_c = \frac{|C_{00}|^2}{|C_{00}|^2 + \sum_{j>0}|C_{j0}|^2}, \tag{3}$$

where $|C_{j0}| = |C_{0k}|$. Note that here we assume that pump photons are in a fundamental Gaussian spatial mode, and that we do not consider temporal or spectral modes. Each signal photon emitted in a fundamental Gaussian mode has an idler partner with an azimuthally symmetric [18] spatial distribution, as required by the conservation of orbital angular momentum [28]. However, there is still freedom in the radial component of the idler spatial mode [29,30]. The basis of the spatial modes onto which the state of the photons is projected during detection depends on the waist of the collection beam [31], which impacts mode overlap and is responsible for the two last terms in Eq. (2).

III. METHODS

A. Experimental setup

The experimental setup is shown in Fig. 2. The cw pump laser outputs a beam with a wavelength of 404 nm, a linewidth of 0.5 nm, and a power of ~80 mW. The linear polarization of the beam is tuned with a half wave plate (HWP). A $4f$ system is used as a spatial filter to obtain a Gaussian pump beam: a $f = 150$-mm focal length lens focuses the light into a pinhole of 0.1 mm in diameter, and a $f = 200$-mm focal lens recovers collimation. Then, a Pellin-Broca prism enhances the purity of the frequency of the pump beam by reflecting parasite wavelengths. We use a manual zoom beam expander (BXZ-355-1-8X, Ronar-Smith) to vary the size of the beam

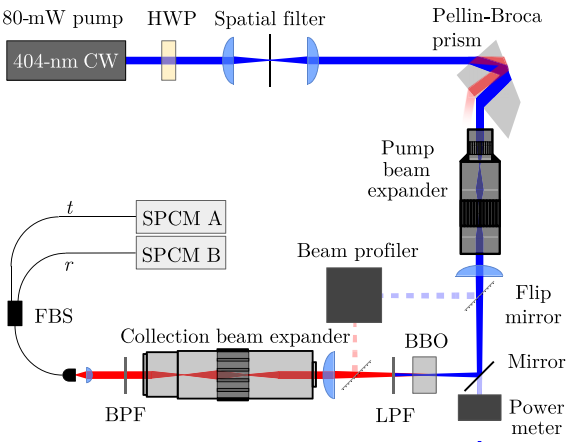

FIG. 2. Experimental setup. The pump beam is launched in free space, passes through a half-wave plate (HWP) followed by a spatial filter, and is reflected by a Pellin-Broca prism, which purifies its spectrum. The beam enters the first beam expander, which modifies its radius, before reaching the focusing lens. A fraction of the light is sent to a power meter, while the beam is focused at the center of the BBO crystal where SPDC photon pairs are generated. The pump is blocked by a long-pass filter (LPF) as the photon pairs are collimated by the detection mode focusing lens and pass through the second beam expander. They are spectrally filtered by a bandpass filter (BPF) and coupled to a single-mode fiber through a lens. The photons are separated by a 50:50 fiber beam splitter (FBS), which has output ports leading to two single-photon counting modules (SPCMs). Flip mirrors are used to easily measure the beam waists by redirecting the light into a beam profiler.

incident on the $f = 500$-mm focusing lens. Owing to this system, the beam waist at the center of the BBO crystal can be engineered continuously from $W_p = 20$ to more than 200 μm. The BBO crystal has a length of $L = 3$ mm and a square aperture of 5×5 mm. A long-pass filter (LPF) is used to block the pump beam after the crystal. The same technique is used to control the beam waist that defines the detection mode: The spot size of the collection beam on the detection focusing lens ($f = 100$ mm for collection beam waists W_c between 8 and 70 μm, and $f = 250$ mm for $W_c = 70$–150 μm) is modified with a variable beam expander (stock No. 87-570, Edmund Optics). A bandpass filter (BPF) with a spectral window of $\Delta\lambda = 10$ nm is inserted in the collinear beam before the light is coupled to a single-mode fiber, and the light is focused with a $f = 18.4$-mm converging lens. Photon pairs are separated by a 50:50 fiber beam splitter (FBS). Two single photon counting modules (SPCMs) (SPCM-AQRH-14-FC, Excelitas Technologies) are used to detect the particles. The count rates are measured from the signal of the detectors by a dual-channel gated photon counter (SR400, Stanford Research Systems). Before and after the crystal, two flip mirrors are positioned equidistantly from the crystal and a beam profiler (BM-7 UV, Coherent), allowing to measure the beam size at the center of the crystal. The collection beam waist is measured by back-propagating 808-nm laser light through the fiber. A power meter (2936-R, Newport) is used to monitor the pump power during the experiment.

TABLE I. Transmittance of the common optical path excluding the BPF T_0, average transmission probability through the BPF of a single photon T_1^{BPF} (and a pair of photons, T_2^{BPF}), see Appendix A. Reflectance r and transmittance t of the FBS, quantum efficiencies of the detectors $\eta_{A,B}$ at 808 nm and noise counts $\mathcal{D}_{A,B}$ of detectors A and B.

T_0 (%)	85.2 ± 0.2
T_1^{BPF} (%)	61.4
T_2^{BPF} (%)	52.5
r (%)	45.9 ± 0.1
t (%)	48.9 ± 0.1
η_A (%)	48.8 ± 0.3
η_B (%)	43.5 ± 0.3
$\mathcal{D}_A$ (cps)	326 ± 19
$\mathcal{D}_B$ (cps)	213 ± 15

B. Transmittance and detection efficiency

The transmission of the common SPDC path (from the crystal to the beam splitter, excluding the BPF) is noted T_0. The average transmission probability through the BPF of a single photon T_1^{BPF} and of a pair of photons T_2^{BPF} are computed separately and require spectral considerations in view of the frequency-dependent transmittance of the bandpass filter (cf. Appendix A). Then, the splitting ratio of the FBS is determined using a 808-nm cw laser diode and the power meter: r and t are the fraction of the input power which is transmitted to each output port of the FBS. The power measurements are performed with an integration time of 1 s and for a duration of several minutes, which is longer than the typical period of fluctuation of the laser power. The uncertainties of the measurements correspond to one standard deviation. Similarly, the quantum efficiencies of the two detectors $\eta_{A,B}$ are measured by comparing the photon flux detected by the SPCMs with the actual incoming rate, itself established with precisely attenuated low-power 808-nm light using neutral density filters. The detection events due to background noise and detector dark counts $\mathcal{D}_{A,B}$ are measured by blocking the SPDC light before the FBS so that the environmental noise is fully taken into account, including the potential impact of any pump light scattered by the optical elements. The measured parameters of the system are given in Table I. Finally, for each measurement, the temporal delay between the coincident detections is increased by delaying the trigger of the signal photon by an amount sufficient to exclude any detection of the paired photon. This enables the measurement of the rate of accidental coincidence counts $\mathcal{N}_{AC}$, attributed to SPDC and background light, or dark counts, and corrections for this effect following Eq. (6). $\mathcal{N}_{AC}$ typically reached values as low as 0.01% of $\mathcal{N}_{A,B}$.

C. Evaluation of correlated-mode coupling efficiency

For each configuration, first, we measure the two experimental parameters for our setup, W_p and W_c, that define the focusing of the beams, which is expressed by the half Rayleigh lengths,

$$Z_{Rj} := \frac{\pi W_j^2}{\lambda_j}, \quad j = p, c, \tag{4}$$

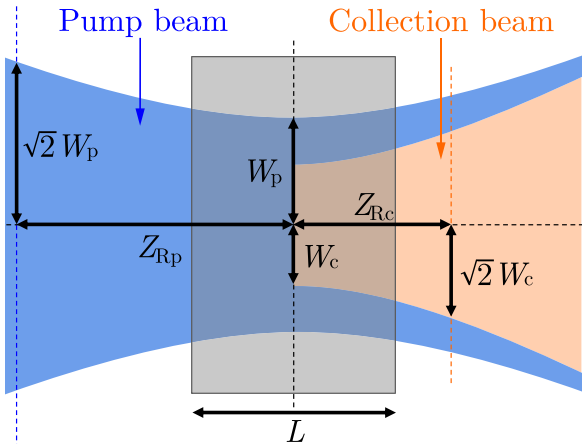

FIG. 3. The pump beam (blue) and collection beam (orange) are focused at the center of the crystal. Their focus is defined by the beam waists W_p, W_c, or, equivalently, by their half Rayleigh lengths Z_{Rp}, Z_{Rc}.

where λ_j is the wavelength of the light traveling in the crystal. The Rayleigh length is commonly compared to the crystal length L (see Fig. 3). Second, a fraction of the pump power is measured with the power meter to monitor in real time the incident pump power on the BBO crystal. This is necessary because the attenuation of the laser power is changed between each measurement for alignment purposes, before to be increased enough to avoid saturation in the detection process. Third, the single count rates $\mathcal{N}_A$, $\mathcal{N}_B$ of each detector as well as the rate of coincidence counts $\mathcal{N}_{CC}$ (detection in a 5-ns window) are measured for a few minutes with an integration time of 1 s. We correct these rates for the noise and accidental counts (see Table I),

$$\begin{aligned} N_A &= \mathcal{N}_A - \mathcal{D}_A, \\ N_B &= \mathcal{N}_B - \mathcal{D}_B, \\ N_{CC} &= \mathcal{N}_{CC} - \mathcal{N}_{AC}. \end{aligned} \tag{5}$$

The probability that a single photon is transmitted to detector A is given by

$$\begin{aligned} 2|C_{00}|^2 \frac{1}{b-a} T_0 \int_b^a d\lambda_s T_{BPF}(\lambda_s)[1 - T_0 t T_{BPF}(\lambda_i)]t \\ +2\sum_{k>0} |C_{0k}|^2 T_0 \frac{1}{b-a} \int_b^a d\lambda_s T_{BPF}(\lambda_s) t, \end{aligned} \tag{6}$$

where $T_{BPF}(\lambda)$ is a fit of the transmission spectrum of the BPF (see Appendix A for details). The first term of Eq. (6) accounts for pairs with both photons in the collection mode, and the second one results from pairs with only one photon in the collection mode. The associated detection probability is η_A. Alternatively, there is a probability

$$|C_{00}|^2 T_0^2 \frac{1}{b-a} \int_b^a d\lambda_s T_{BPF}(\lambda_s) T_{BPF}(\lambda_i) t^2 \tag{7}$$

that a pair of photons reach detector A, in which case the detection event probability is $2\eta_A - \eta_A^2$. Substituting $t \to r$ in Eqs. (6) and (7) and replacing η_A by η_B yields the probabilities for detector B. Experimentally, we only detect single-mode photons, and, thus, we cannot measure the total rate of emitted pairs N, nor the true probabilities of emission in the different states of Eq. (2). We simply introduce the rate of "collectable" pairs as

$$N_{00} := N|C_{00}|^2, \tag{8}$$

as well as the rate of pairs with the signal photon in the detection mode and the idler photon in a higher-order mode, given as

$$N_{0+} := N \sum_{k>0} |C_{0k}|^2. \tag{9}$$

The operational expression for the correlated-mode coupling efficiency (3) is then given by

$$\eta_c = \frac{N_{00}}{N_{00} + N_{0+}}. \tag{10}$$

To lighten the notation, we note T_1^{BPF} the average probability for a single photon to be transmitted through the BPF, Eq. (A2), and T_2^{BPF} the average probability for a pair to be transmitted through the BPF, Eq. (A3). Considering Eqs. (6) and (7) and their associated detection probabilities, the rates of Eq. (6) are expected to be

$$\begin{aligned} N_A = N_{00}\left(2T_0 T_1^{BPF} t\eta_A - T_0^2 T_2^{BPF} t^2 \eta_A^2\right) \\ +2N_{0+} T_0 T_1^{BPF} t\eta_A, \end{aligned} \tag{11}$$

$$\begin{aligned} N_B = N_{00}\left(2T_0 T_1^{BPF} r\eta_B - T_0^2 T_2^{BPF} r^2 \eta_B^2\right) \\ +2N_{0+} T_0 T_1^{BPF} r\eta_B, \end{aligned} \tag{12}$$

and

$$N_{CC} = 2N_{00} T_0^2 T_2^{BPF} rt\eta_A\eta_B. \tag{13}$$

From there, Eq. (13) is inverted to find N_{00}, which is in its turn injected into Eqs. (11) and (12), giving two estimations N_{0+}^A, N_{0+}^B, which are averaged as $N_{0+} = \frac{N_{0+}^A + N_{0+}^B}{2}$. Equation 10 provides the resulting operational formula for the correlated-mode coupling efficiency,

$$\eta_c = \frac{4N_{CC} T_1^{BPF}}{T_0 T_2^{BPF}[\eta_A t(2N_B + N_{CC}) + \eta_B r(2N_A + N_{CC})]}. \tag{14}$$

IV. RESULTS

A. Effect of detection focus on correlated-mode coupling efficiency

We investigated three different pump focusing situations, namely, $W_p = (51 \pm 2)$, (127 ± 3) and (208 ± 3) μm for which the collection beam waist continuously ranged from 8 to 150 μm, and Eq. (10) yielded the experimental correlated-mode coupling efficiency. Before each measurement, the fiber position was carefully optimized in order to measure the maximal η_c reachable with the current focusing condition. Figure 4 shows η_c as a function of Z_{Rc}/L for three different focusing conditions of the pump beam. Note that we do not show the error bars along the abscissa on the graphs and plot only the region $Z_{Rc}/L < 10$ for the sake of readability. The numerical simulations (lines) are taken from Ref. [18];

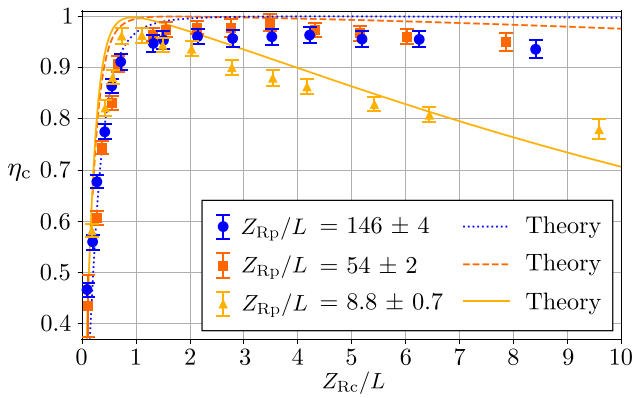

FIG. 4. Correlated-mode coupling efficiency η_c as a function of the Rayleigh length of the collection mode Z_{Rc} expressed as a multiple of crystal length L. The maximum value of η_c was comparable for the three pump beam configurations. The error bars represent one standard deviation. The theoretical curves were computed with Eq. (B1).

see Appendix B for details. The overall patterns are in good agreement with the experimental data. It can be seen that the maximum efficiencies for each pump focus are comparable, but each was achieved with a different detection setting. There also appears to be a detection focus for which all pump configurations enabled efficient coupling (around $Z_{Rc}/L = 1$). For tight pump focusing, high coupling efficiency is only possible if $Z_{Rc}/L = 1$ [Fig. 4, yellow (light gray) triangles], and for looser collection focusing, η_c drops significantly. Note that there is a systematic drop in η_c when the Rayleigh length of the collection beam is smaller than the crystal length; this can easily be interpreted as the consequence of a reduction of the interaction volume (the overlap between the collection beam, the pump and the crystal). In quantifying the brightness of the source via the rate of coincidence counts, we observed that it strongly depends on the focus of the pump beam. Comparing Figs. 4 and 5, it can be seen that for each pump configuration, choosing a focusing condition for the collection beam to optimize brightness will also optimize the coupling efficiency and

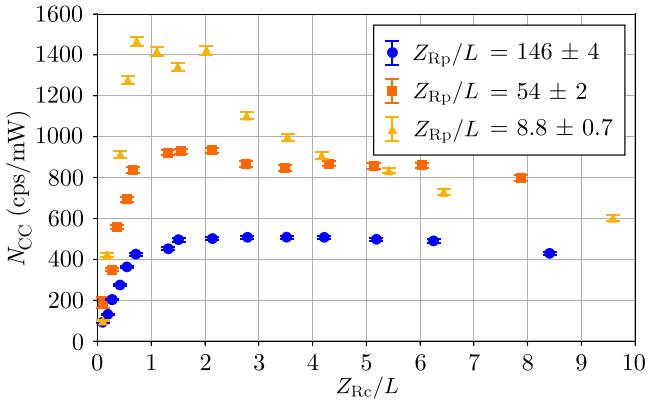

FIG. 5. Brightness of the source N_{CC} in coincidence counts per second for different configurations as a function of the Rayleigh length of the collection mode over the crystal length Z_{Rc}/L. The error bars represent one standard deviation.

TABLE II. Maximum correlated-mode coupling efficiency η_c and heralding ratio $\eta_{s,i}$ for each pump focus, brightness $N_{CC} = \mathcal{N}_{CC} - \mathcal{N}_{AC}$ obtained for each pump focus, and associated power incident on the crystal. The numerical aperture (NA) for the pump focus is given by NA $= n \sin\theta$ where θ is the divergence half-angle of the pump beam.

W_p (μm)	51 ± 2	127 ± 3	208 ± 3
Z_{Rp} (mm)	26 ± 2	163 ± 7	438 ± 11
NA ($\times 10^{-3}$)	3.3 ± 0.1	1.32 ± 0.03	0.80 ± 0.01
Optimal W_c (μm)	21 ± 2	45 ± 2	50 ± 2
η_c (%)	95.9 ± 1.4	98.4 ± 1.6	95.8 ± 1.5
η_s (%)	17.1 ± 0.3	17.6 ± 0.3	17.2 ± 0.3
η_i (%)	16.0 ± 0.3	16.4 ± 0.3	15.9 ± 0.3
N_{CC} ($s^{-1}mW^{-1}$)	1416 ± 21	848 ± 13	508 ± 8
Power (mW)	3.318 ± 0.004	4.448 ± 0.006	7.291 ± 0.008

vice versa. Our data suggest that in order to jointly optimize both N_{CC} and η_c, Z_{Rc}/L must be near unity, and the pump beam should be tightly focused. For tight pump focusing, which provides high brightness, high correlated-mode coupling efficiency is still possible, but demands fine-tuning of the collection beam focus. The heralding ratios

$$\eta_i = \frac{N_{CC}}{N_A}, \quad \eta_s = \frac{N_{CC}}{N_B}, \tag{15}$$

and the brightness of the source are given for the optimal point of each pump focus in Table II. Note that in this section, the brightness is expressed as a fraction of the pump power to be able to observe its pattern as a function of the focusing conditions. The incident pump power associated to data of Fig. 5 ranged from 2.6 to 6.8, 3.5 to 9.8, and 7.2 to 15.5 mW, respectively, for the tight, medium, and loose pump focusing.

B. Effect of pump focus on correlated-mode coupling efficiency

In the tightly focused collection beam region, the rate of coincidence counts increases as the pump is more tightly focused. This effect can be understood as a consequence of the enhancement of the absolute fiber coupling rate due to weak spatial entanglement of the photon pairs [32]. However, this is not the case for every collection beam size, as shown in Fig. 5. To illustrate this fact, and to test the limits of our source by tightening the pump focus to achieve higher brightness, we varied W_p continuously from 20 to 200 μm, for the collection parameters $Z_{Rc}/L = 1.18 \pm 0.16$ and $Z_{Rc}/L = 8.53 \pm 0.47$. The observed coupling efficiency and brightness are shown together in Fig. 6. In accordance with Fig. 4, the maximum correlated-mode coupling efficiency is limited as the focus of the pump tightens, and this effect is enhanced for loose detection focusing. In fact, we observed that the efficiency drops if $W_p \lesssim 2W_c$, i.e., $Z_{Rp} \lesssim 8Z_{Rc}$. The physical reason for this limited mode matching is more subtle than the one observed in Fig. 4 when the detection focus tightens. However, we note that this effect appears in the numerical simulations, up to some discrepancy (see Appendix B). The overall maximum correlated-mode coupling efficiency reached in this experiment is $\eta_c = (99.0 \pm 1.3)\%$, visible on Fig. 6 for $Z_{Rc}/L = 1.18 \pm 0.16$ and $Z_{Rp}/L = 80 \pm 3$. The

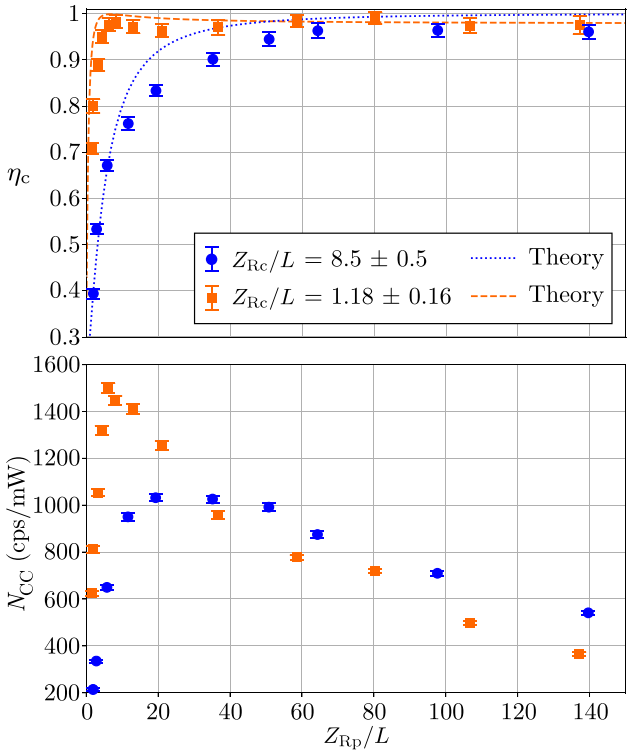

FIG. 6. Correlated-mode coupling efficiency η_c and brightness N_{CC} as a function of the Rayleigh length of the pump over the crystal length Z_{Rp}/L for two configurations of the collection beam: strong [orange (gray) squares] and medium [blue (dark gray) circles] focus. The error bars represent one standard deviation and the theoretical approximation of η_c is given by Eq. (B1).

data show that the brightness exhibits a maximum for a specific value of pump focus (Fig. 6, bottom). Note that the error bars were removed for brightness as they are too small with respect to the markers. As the focus of the collection beam tightens, the peak of the brightness curve gets sharper and is displaced towards stronger pump focusing. For a tightly focused collection beam, the maximum brightness is reached in the region of maximum coupling efficiency, giving rise to jointly optimized correlated-mode coupling efficiency and brightness for $Z_{Rc}/L = 1.18 \pm 0.16$: $\eta_c = (98.3 \pm 1.4)\%$, $N_{CC} = (1450 \pm 20)\ \mathrm{s}^{-1}\,\mathrm{mW}^{-1}$ observed for $Z_{Rp}/L = 8.1 \pm 0.7$ (pump power $3.638\ \mathrm{mW} \pm 0.001\ \mathrm{mW}$) and $\eta_c = (97.6 \pm 1.3)\%$, $N_{CC} = (1500 \pm 20)\ \mathrm{s}^{-1}\,\mathrm{mW}^{-1}$ observed for $Z_{Rp}/L = 6.1 \pm 0.6$ (pump power $3.443\ \mathrm{mW} \pm 0.002\ \mathrm{mW}$), which are close to the overall optimal conditions for our source. The data reported in Fig. 6 was measured with incident powers ranging from 3.3 to 15 and 2.2 to 7.1 mW, for tightest and loosest collection focusing, respectively.

To summarize, we have found: (1) the correlated-mode coupling efficiency can be very close to unity for any pump focus, however, the optimal Rayleigh length of the collection mode Z_{Rc} depends on the pump focus parameter Z_{Rp}, and (2) the flux of the photon pairs coupled to the fibers (brightness) can be large for tight pump focusing (small Z_{Rp}), but Z_{Rc} needs to be precisely adjusted to the optimal value with very small redundancy. Thus, for the case the brightness can be compensated by a larger pump power, some larger Z_{Rp} may be preferred in order to achieve very high correlated-mode coupling efficiency.

V. CONCLUSION

We experimentally investigated the focusing constraints on the correlated-mode coupling efficiency into single-mode fibers of degenerated photon pairs generated by collinear type-I SPDC in a bulk BBO crystal. With this configuration, we demonstrated the behavior of η_c with respect to the focusing strength of the pump and collection beams, allowing the correlated-mode coupling efficiency to be pushed close to 100% for different focusing conditions. Additionally, we reported an experimental optimization of correlated-mode coupling efficiency for SPDC sources using type-I phase matching, confirming for this case the possibility of reaching high η_c in the same way that has been previously demonstrated for type-II phase matching [13]. The maximum correlated-mode coupling efficiency we observed was $\eta_c = (99.0 \pm 1.3)\%$. Our experiment elucidates the evolution of the correlated-mode coupling efficiency and brightness as a function of the focusing conditions and clarifies the optimal parameters to jointly enhance both features. It was found that the optimal settings that maximize both η_c and N_{CC} is when the Rayleigh length of the collection beam equals the crystal length, and the Rayleigh length of the pump beam is about eight times longer. It was shown that strong pump focusing still allows high coupling efficiency while giving maximum brightness, although a stringent constraint on the collection beam waist size is required. We observed that the optimal coupling efficiency and brightness are obtained for the same detection focus, whereas this is the case for the pump focus only when the Rayleigh length of the collection beam is close to the crystal length. Parametric fluorescence using type-I phase matching is still widely used in various works (for example, Ref. [20]), and the results shown here can directly benefit them. Furthermore, the results can be, in principle, applied to other phase-matching conditions.

The study of correlated-mode coupling efficiency gives an appreciation of the performance of the source, regardless of the transmittance of the setup components. It is exclusively based on spatial mode matching between the emitted photon pairs and the collected mode. Hence, it is a fundamental and relevant metric that can be defined in various situations, and its optimization is crucial in order to achieve high collection efficiency of photon pairs and heralding ratios. We believe that this paper will be informative for experimentalists and help to find optimal performance in future experiments harnessing SPDC light as well as in further optimization studies. We are interested in extending this research to broadband spectra and different types of phase matching.

ACKNOWLEDGMENTS

We sincerely thank Professor Dr. C. Galland, Dr. T. Kiyohara, Dr. B. Cao, and M. Arahata for useful discussions and comments on our work. This work was supported, in part, by JST CREST Grant No. JPMJCR1674, Japan, MEXT Quantum Leap Flagship Program (MEXT Q-LEAP)

Grant No. JPMXS0118067634, JST-PRESTO (Grant No. JPMJPR15P4), and KAHENHI Grants-in-Aid No. 21H04444.

N.S. and G.P. contributed equally to this work.

APPENDIX A: BI-PHOTON TRANSMISSION PROBABILITY

Among the optical elements in the common SPDC path, namely, from the crystal to the beam splitter, the bandpass filter is the only one to have a frequency-dependent transmittance. SPDC photons of one pair are tightly linked by the energy conservation relation,

$$\omega_{\mathrm{i}} = \omega_{\mathrm{p}} - \omega_{\mathrm{s}}, \tag{A1}$$

where ω_{p}, ω_{s}, and ω_{i} are the respective frequencies of the pump, signal, and idler photons. As a consequence, even for a symmetric transmission spectrum, since the smoothly decreasing (over about 2 nm, see Fig. 7) edges of the spectrum of the BPF are included in the broad spectrum of degenerated SPDC pairs (the spectral distribution of down-converted light in our setup has a full width at half maximum of approximately 60 nm, typical of type-I sources), the transmission probability for a pair through the BPF is different from the square of the probability of transmission for a single photon. The transmission spectrum of the BPF was measured with a spectrometer (SR500i-E1, Andor) equipped with a charge-coupled device (DU 416, iDus), while using collinear degenerated SPDC light produced in the BBO crystal as a source, coupled to a multimode fiber (assuming that inserting the BPF does not disturb the coupling to the fiber) and sent to the spectrometer. By fitting the transmittance curve (Fig. 7) with a series expansion $T_{\mathrm{BPF}}(\lambda)$, one can compute the transmission probability of one photon through the BPF as

$$T_1^{\mathrm{BPF}} = \frac{1}{b-a}\int_b^a d\lambda\, T_{\mathrm{BPF}}(\lambda), \tag{A2}$$

and the transmission probability for a pair of photons,

$$T_2^{\mathrm{BPF}} = \frac{1}{b-a}\int_b^a d\lambda_{\mathrm{s}} T_{\mathrm{BPF}}(\lambda_{\mathrm{s}}) T_{\mathrm{BPF}}(\lambda_{\mathrm{i}}), \tag{A3}$$

where a and b are the wavelengths bounding the integration range. Note that following Eq. (A1), the wavelengths of the signal and idler photons are linked by

$$\lambda_{\mathrm{i}} = \left(\frac{1}{\lambda_{\mathrm{p}}} - \frac{1}{\lambda_{\mathrm{s}}}\right)^{-1}. \tag{A4}$$

The noise during spectrum measurement was estimated by measuring the transmittance outside the BPF window, which had a mean value of $\overline{T} = 2.36 \times 10^{-5}$ and a standard deviation (noise) of $\sigma = 2.25 \times 10^{-4}$. The experimental boundaries a and b correspond to a transmittance of 5σ. The transmittance T_0 of the remaining optics was measured by backpropagating 808-nm light through the FBS, and recording the ratio between the input and output powers.

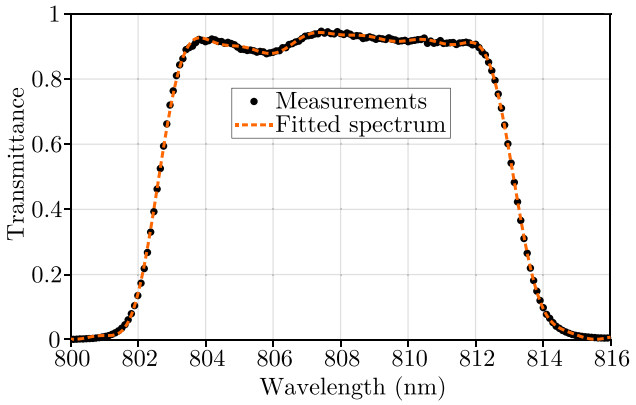

FIG. 7. Transmission spectrum of the bandpass filter, fitted by an eight-term Fourier series expansion $T_{\mathrm{BPF}}(\lambda)$.

APPENDIX B: THEORETICAL APPROXIMATION

The theoretical prediction of Bennink [18] was compared to our measurements in Figs. 4 and 6. In his derivation, various assumptions were used, and he stressed that the predictions of his theoretical model may be limited for some sources, including type-I phase matching. However, we observed that this model was still able to predict the optimal parameters that enable high efficiency. Keeping the notation of Ref. [18], the correlated-mode coupling efficiency can be expressed as

$$\eta_{\mathrm{c}} = \frac{P_{\mathrm{s}}(0)}{P_{\mathrm{s}}(\infty)}, \tag{B1}$$

where

$$P_{\mathrm{s}}(m) = \int_{\omega_{\mathrm{a}}}^{\omega_{\mathrm{b}}} \sum_{n=0}^{m} |\psi_n(\omega_{\mathrm{s}}, \omega_{\mathrm{i}})|^2 d\omega_{\mathrm{s}} d\omega_{\mathrm{i}} \tag{B2}$$

is the probability that the signal photon is in the detection mode (0), considering that the idler photon can be emitted in the range of discrete spatial modes $[0, m]$. Equation (B2) is an integral with respect to the signal and idler frequencies $\omega_{\mathrm{s}}, \omega_{\mathrm{i}}$, which we computed for the range given by our BPF $[\omega_a, \omega_b]$. $\psi_n(\omega_{\mathrm{s}}, \omega_{\mathrm{i}})$ is the SPDC amplitude associated with the nth idler mode (see Ref. [18] for a detailed derivation and relevant approximations). Although the theory correctly predicts the location of the maximum correlated-mode coupling efficiency, the experimental values are systematically slightly lower than predicted. We believe that this is due to theoretical assumptions that are not satisfied by our system.

[1] S. E. Harris, M. K. Oshman, and R. L. Byer, Phys. Rev. Lett. **18**, 732 (1967).

[2] D. N. Klyshko, Sov. J. Quantum Electron. **7**, 591 (1977).

[3] P. G. Kwiat, A. M. Steinberg, R. Y. Chiao, P. H. Eberhard, and M. D. Petroff, Appl. Opt. **33**, 1844 (1994).

[4] I. Shoji, T. Kondo, A. Kitamoto, M. Shirane, and R. Ito, J. Opt. Soc. Am. B **14**, 2268 (1997).

[5] D. C. Burnham and D. L. Weinberg, Phys. Rev. Lett. **25**, 84 (1970).
[6] A. Soujaeff, T. Nishioka, T. Hasegawa, S. Takeuchi, T. Tsurumaru, K. Sasaki, and M. Matsui, Opt. Express **15**, 726 (2007).
[7] M. Tchoffo and A. Tene, Chaos, Solitons Fractals **140**, 110110 (2020).
[8] A. F. Abouraddy, M. B. Nasr, B. E. A. Saleh, A. V. Sergienko, and M. C. Teich, Phys. Rev. A **65**, 053817 (2002).
[9] T. Ono, R. Okamoto, and S. Takeuchi, Nat. Commun. **4**, 2426 (2013).
[10] J. Carolan, C. Harrold, C. Sparrow, E. Martín-López, N. J. Russell, J. W. Silverstone, P. J. Shadbolt, N. Matsuda, M. Oguma, M. Itoh, G. D. Marshall, M. G. Thompson, J. C. F. Matthews, T. Hashimoto, J. L. O'Brien, and A. Laing, Science **349**, 711 (2015).
[11] H.-S. Zhong, Y.-H. Deng, J. Qin, H. Wang, M.-C. Chen, L.-C. Peng, Y.-H. Luo, D. Wu, S.-Q. Gong, H. Su, Y. Hu, P. Hu, X.-Y. Yang, W.-J. Zhang, H. Li, Y. Li, X. Jiang, L. Gan, G. Yang, L. You, Z. Wang, L. Li, N.-L. Liu, J. J. Renema, C.-Y. Lu, and J.-W. Pan, Phys. Rev. Lett. **127**, 180502 (2021).
[12] X.-L. Wang, L.-K. Chen, W. Li, H.-L. Huang, C. Liu, C. Chen, Y.-H. Luo, Z.-E. Su, D. Wu, Z.-D. Li, H. Lu, Y. Hu, X. Jiang, C.-Z. Peng, L. Li, N.-L. Liu, Y.-A. Chen, C.-Y. Lu, and J.-W. Pan, Phys. Rev. Lett. **117**, 210502 (2016).
[13] P. B. Dixon, D. Rosenberg, V. Stelmakh, M. E. Grein, R. S. Bennink, E. A. Dauler, A. J. Kerman, R. J. Molnar, and F. N. C. Wong, Phys. Rev. A **90**, 043804 (2014).
[14] F. Kaneda and P. G. Kwiat, Sci. Adv. **5**, eaaw8586 (2019).
[15] C. Kurtsiefer, M. Oberparleiter, and H. Weinfurter, Phys. Rev. A **64**, 023802 (2001).
[16] D. Ljunggren and M. Tengner, Phys. Rev. A **72**, 062301 (2005).
[17] A. Ling, A. Lamas-Linares, and C. Kurtsiefer, Phys. Rev. A **77**, 043834 (2008).
[18] R. S. Bennink, Phys. Rev. A **81**, 053805 (2010).
[19] H. E. Guilbert and D. J. Gauthier, IEEE J. Sel. Top. Quantum Electron. **21**, 215 (2015).
[20] A. Sansa Perna, E. Ortega, M. Gräfe, and F. Steinlechner, Appl. Phys. Lett. **120**, 074001 (2022).
[21] D. J. Saunders, A. J. Bennet, C. Branciard, and G. J. Pryde, Sci. Adv. **3**, e1602743 (2017).
[22] Q. Zeng, J. Shang, H. C. Nguyen, and X. Zhang, Phys. Rev. Res. **4**, 013151 (2022).
[23] T. Kiyohara, R. Okamoto, and S. Takeuchi, Opt. Express **25**, 32443 (2017).
[24] T. Kiyohara, N. Yamashiro, R. Okamoto, H. Araki, J.-Y. Wu, H. F. Hofmann, and S. Takeuchi, Optica **7**, 1517 (2020).
[25] T. Kiyohara, R. Okamoto, and S. Takeuchi, Opt. Express **28**, 17490 (2020).
[26] Y. Mukai, M. Arahata, T. Tashima, R. Okamoto, and S. Takeuchi, Phys. Rev. Appl. **15**, 034019 (2021).
[27] J. P. Villabona-Monsalve, O. Calderón-Losada, M. Nuñez Portela, and A. Valencia, J. Phys. Chem. A **121**, 7869 (2017).
[28] S. Franke-Arnold, S. M. Barnett, M. J. Padgett, and L. Allen, Phys. Rev. A **65**, 033823 (2002).
[29] F. M. Miatto, A. M. Yao, and S. M. Barnett, Phys. Rev. A **83**, 033816 (2011).
[30] V. D. Salakhutdinov, E. R. Eliel, and W. Löffler, Phys. Rev. Lett. **108**, 173604 (2012).
[31] E. Karimi, D. Giovannini, E. Bolduc, N. Bent, F. M. Miatto, M. J. Padgett, and R. W. Boyd, Phys. Rev. A **89**, 013829 (2014).
[32] W. P. Grice, R. S. Bennink, D. S. Goodman, and A. T. Ryan, Phys. Rev. A **83**, 023810 (2011).